JMEPEG (2011) 20:65–70
DOI: 10.1007/s11665-010-9645-x

1059-9495/$19.00

Macrosegregation Behavior of Ti-10V-2Fe-3Al Alloy During Vacuum Consumable Arc Remelting Process

Zhijun Yang, Hongchao Kou, Jinshan Li, Rui Hu, Hui Chang, and Lian Zhou

(Submitted December 16, 2009; in revised form March 8, 2010)

The effects of melting current and magnetic field in vacuum consumable arc remelting (VAR) process on the macrosegregation of Ti-10V-2Fe-3Al ingot are investigated in this paper. The results show that Fe content increases gradually from the bottom to the top of ingots along axial direction and the degree of macrosegregation is greater in the radial direction in the middle of the ingot versus the top and bottom. The macrosegregation rate of Fe element is higher with melting current of 2.6 kA than that of 1.7 kA in Ti-10V-2Al-3Fe ingot. There are two forces, buoyancy and Lorentz forces which arise from the flow of current through the pool of VAR when without magnetic stirring, but a new Lorentz force arising from the presence of external inductors occurs with adding magnetic stirring which decreases the macrosegregation rate of Fe element in Ti-10V-2Fe-3Al.

Keywords fluid motion, macrosegregation, solute partitioning, Ti-10V-2Fe-3Al alloy, VAR

1. Introduction

The Ti-10V-2Fe-3Al ingots from vacuum consumable arc remelting (VAR) process are used typically as a material for critical parts of jet engines and industrial gas turbines as well as in military application (Ref 1-3). The specification of application often demands outstanding material properties (Ref 4, 5). Despite many years of research and development of VAR process of Ti-10V-2Fe-3Al alloy, there are still many challenges in making defect-free and high-quality ingots (Ref 6, 7), such as, LDI and HDI defects, beta flecks and macrosegregation (Ref 8-11). In which, macrosegregation is an inhomogeneous distribution of alloying elements that is result from two physical phenomena, solute partitioning and fluid flow during the remelting process (Ref 12, 13). The fundamental reason for segregation is the partitioning of solute elements between liquid and solid phases during solidification process. Partitioning by itself results in a microscale redistribution of solute between solid and liquid phase at the solid-liquid interface during alloy solidification. In the case of Ti-10V-2Fe-3Al alloy, the liquid phase is enriched and the solid phase is depleted of solute elements, such as Fe, C, Si etc. The so-called partition coefficient ($K = C_S/C_L$) of these elements is less than unity, meaning that the concentration of the element in the solid phase is less than in the liquid. In the case of elements with $K > 1$, e.g. Al, N, O, the solid phase becomes enriched during solidification. Meanwhile, the other main reason of segregation is the relative movement of liquid and solid phases in the two-phase zone of the melting.

The major segregating element for Ti-10V-2Fe-3Al alloy is Fe, which leads to form beta flecks which have a significant effect on mechanical properties of Ti-10V-2Fe-3Al alloy. In order to obtain a sound ingot, it is necessary to understand the rule of solute partitioning and control the processing parameters which affect the pool profile and as-cast structure during VAR process. Accordingly, the macrosegregation behaviors of Ti-10V-2Fe-3Al ingots are investigated in this paper, which including the effect of VAR parameters, such as melting current and magnetic field, on fluid motion in the molten pool and macrostructure of ingots. At last, the formation mechanism of macrosegregation is discussed and some effective methods for reducing segregation of this alloy are produced.

2. Experimental Procedures

The test materials were produced through twice melting vacuum consumable arc remelting. Firstly, Φ 60 × 100 mm ingots of Ti-10V-2Fe-3Al which were used as consumable electrode for twice remelting were made by VAR from compacted sponge titanium. Then a lot of ingots (Φ 100 × 140 mm, 6.5 kg) of Ti-10V-2Fe-3Al were produced by twice VAR. The ingot and electrode diameters and process parameters for the individual stages are given in Table 1, in which, ingot A and ingot B was carried out with relatively weak melting current (1.7 kA) and operated without and with magnetic field respectively. Ingot C and D were carried out with relatively strong melting current (2.6 kA) and operated without and with magnetic field respectively too. Three ingots for each scenario (A, B, C and D) were produced in this study and the results were found to be consistent.

The ingots were split along the center of axis for the chemical composition analysis. As shown in Fig. 1, the test samples were cut from the ingots along the central column of the longitudinal section (Fig. 1a) and the radial lines of the

Zhijun Yang, Hongchao Kou, Jinshan Li, Rui Hu, Hui Chang, and **Lian Zhou**, State Key Laboratory of Solidification Processing, Northwestern Polytechnical University, Xi'an 710072, China. Contact e-mail: yzj165@163.com.

Table 1 Process parameter and diameters for two VAR stage

VAR Stage	Number	Voltage, V	I_{arc}, kA	Magnetic intensity, T	Vacuum pressure, Pa	Average melt rate, g/s	$D_{electrode}$, m	D_{ingot}, m
1	…	23	1.1	0.003	1.0×10^{-3}	9.4	0.03	0.06
2	Ingot A	26	1.7	0	1.2×10^{-3}	14.1	0.06	0.1
2	Ingot B	26	1.7	0.004	1.2×10^{-3}	16.1	0.06	0.1
2	Ingot C	26	2.6	0	1.2×10^{-3}	18.8	0.06	0.1
2	Ingot D	26	2.6	0.004	1.2×10^{-3}	21.5	0.06	0.1

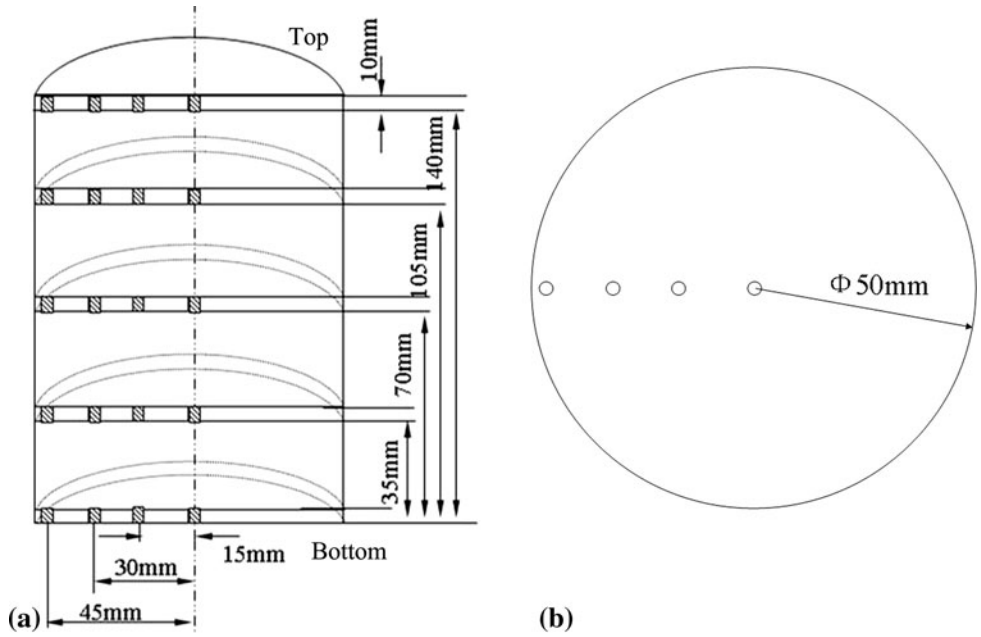

Fig. 1 Position of ingot sampling: (a) longitudinal section of ingot and (b) cross section of ingot

cross section (Fig. 1b). Then the samples of the hatched areas were analyzed by chemical composition analysis technique and the macrosegregation results were found to be consistent by repeatable chemical composition analysis. Finally the typical macrostructure morphology of longitudinal section of ingots was observed by camera.

3. Results and Discussion

3.1 Macrosegregation of Ti-10V-2Fe-3Al During Different Solidification Process of VAR

The axial and radial distribution of Fe element at different sections of the alloy ingot A is shown in Fig. 2. It can be seen from Fig. 2a that the Fe content gradually increases along the central axis from the bottom to the top of the ingot. Figure 2(b) shows the radial direction distribution of Fe element at sections of the bottom, middle and top of ingot A respectively. It can be seen that Fe content gradually increases from the edge to the center of the ingot. The degree of macrosegregation is smaller in the radial direction at the top and bottom of ingot A versus the middle. This phenomenon is also observed in other ingot.

Under VAR conditions, the classical theory of partition coefficient show as (Ref 14):

$$C = C_0(1 - \xi)^{K-1} \quad \text{(Eq 1)}$$

where C is the concentration of solute element dissolved at every moment, C_0 is the initial concentration of solute element, ξ is the volume fraction of solidified part, and K is the partition coefficient of solute element.

The partition coefficient K is defined as the ratio between concentrations of solid and liquid phases in equilibrium condition. Binary phase diagram reveals approximate partition coefficients for the three binary systems $K^{\text{Ti-V}} \sim 1.0$, $K^{\text{Ti-Fe}} \sim 0.28$, $K^{\text{Ti-Al}} \sim 1.23$ for Ti-V, Ti-Fe and Ti-Al binary dilute systems respectively, in which $K^{\text{Ti-V}}$ is close to 1, indicating that V is not expected to appreciably segregation during VAR of Ti-10V-2Al-3Fe alloy. But the $K^{\text{Ti-Fe}}$ and $K^{\text{Ti-Al}}$ deviate from 1, portending microscale segregation of Al and Fe. It is noticeable that the partition coefficient of Fe is far less than 1, signifying its preference into residual liquid, therefore, Fe content gradually increases along the axis direction from the bottom to the top of ingots which is coincident with the solidification sequence of Ti-10V-2Fe-3Al ingots.

In the practical VAR solidifying process, K is not a constant, it depends much on solidifying velocity. The partition coefficient

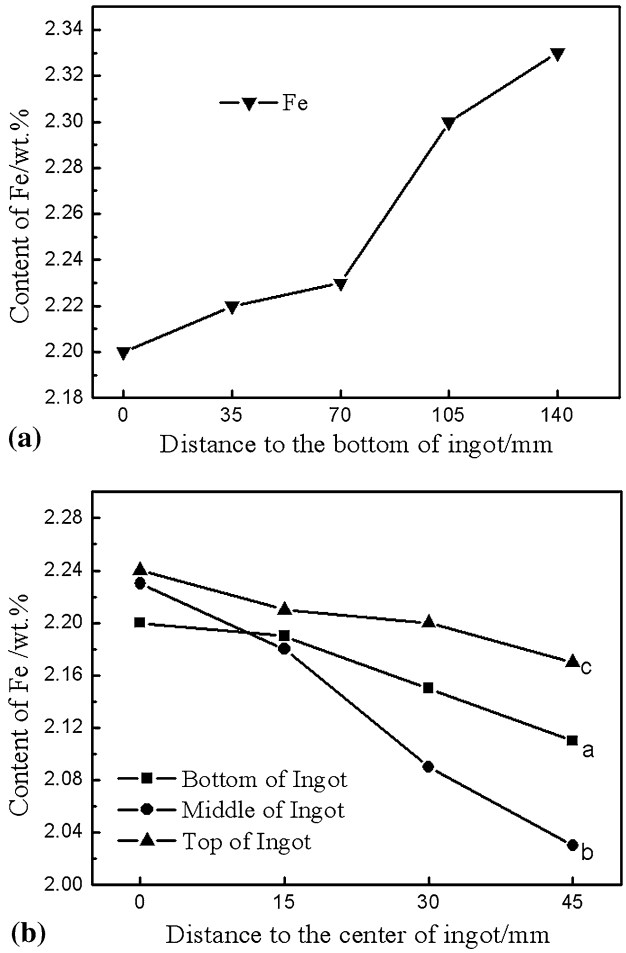

Fig. 2 The distribution of Fe element in the different section: (a) axial direction and (b) radial direction

in practical process can be expressed as K_a, the relationship between K_a and K_0 is shown in the equation (Ref 14):

$$K_a = K_0 + (1 - K_0)\exp(-D_i/R\delta) \quad \text{(Eq 2)}$$

where D_i is the diffusion coefficient of interface; R is the solidifying velocity, δ is the thickness of atom layer along the solidifying direction. According to the equation, the higher the R is, the K_a is more nearly to 1. The lower the R is, the K_a is more nearly to K_0.

Figure 3 shows the typical macrostructure of longitudinal section of the ingot A. The crystalline grains at the bottom of the ingot grow upwards along the whole bottom cross section, as shown in Fig. 3(a zone). The heat dissipation along axial direction is much larger than that of radial direction, so the cooling intensity and solidifying velocity are higher and the K is close to 1, i.e., the radial solidifying segregation at the bottom of the ingot is very small. Along with the remelting evolution, the depth of molten pool also increases gradually with the height of solidified ingot increasing. Therefore, the axial heat dissipation gradually become more difficult and the radial heat dissipation becomes dominant, which results in the crystallization growth direction at the edge of ingots pointing to the center, as seen in Fig. 3(b zone). At the same time, the solidifying velocity R and K decrease. So the enrichment of Fe element in the center of ingots results in the increase of the macrosegregation degree. At the end of VAR, the melting

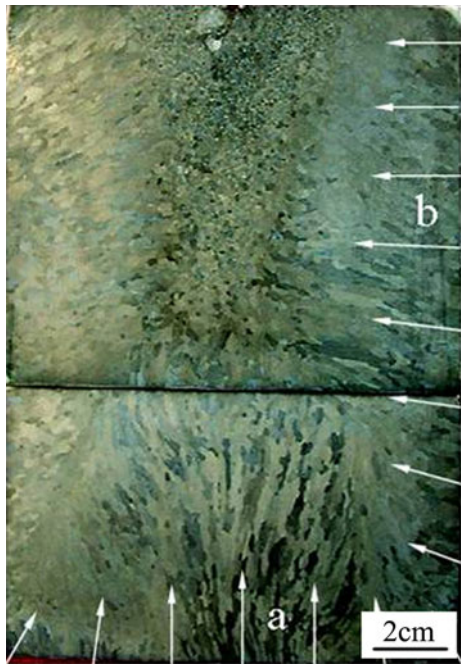

Fig. 3 Macrostructure of ingot A along longitudinal section

current suddenly dropped, which leads to the solidifying velocity increases greatly (Ref 15-17) and, therefore, the macrosegregation degree of Fe element decreases at the end of the whole solidification process.

3.2 Influence of Remelting Current on the Macrosegregation of Ti-10V-2Fe-3Al

Different macrosegregation rates have been frequently reported as an indication of segregation severity. Macrosegregation rate (σ_m) is adequate to be employed with a large number of microanalyses at random points, as shown by:

$$\sigma_m = \frac{1}{nc_0}\sum_{i=1}^{n}|c_i - c_0| \times 100\% \quad \text{(Eq 3)}$$

where n is the total number of microanalyses in the section, c_i is the element content for each microanalysis and c_0 is the average element content of all microanalyses in the section. The effect of melting current on macrosegregation rate of Fe element in Ti-10V-2Fe-3Al alloy is shown in Fig. 4. It can be seen that the macrosegregation rate increases firstly and then decreases along axial direction from the bottom to the top of the ingots. In addition, the macrosegregation rate of Fe element is higher with melting current of 2.6 kA than that of 1.7 kA. It can be concluded that the macrosegregation rates of alloy elements are significantly affected by the melting current in Ti-10V-2Fe-3Al alloy.

Without regard to magnetic stirring in VAR process, there are at least two competing sources of motion in the molten pool. One is buoyancy, the cases with weak clockwise flow cell, which develops in the vicinity of the side of the forming ingot (Ref 18). The buoyancy in the pool is expected as:

$$F_f = -\rho g\beta(T - T_M) \quad \text{(Eq 4)}$$

where β is the expansion coefficient, T is the surface temperature of pool and T_M is the melting point of ingot. The surface

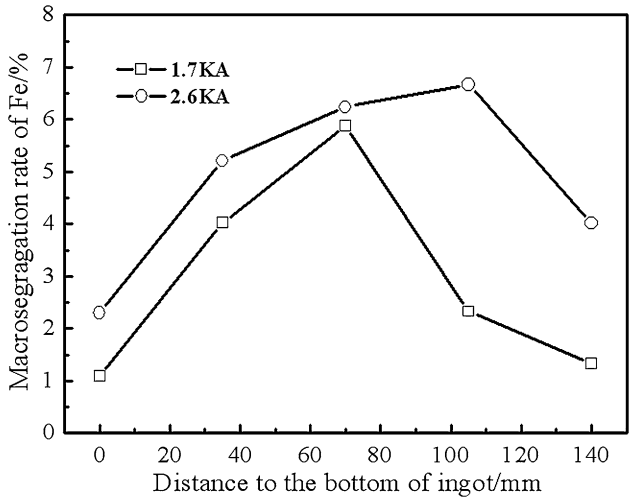

Fig. 4 Effect of melting current on macrosegregation rate of Fe in the ingots A and B

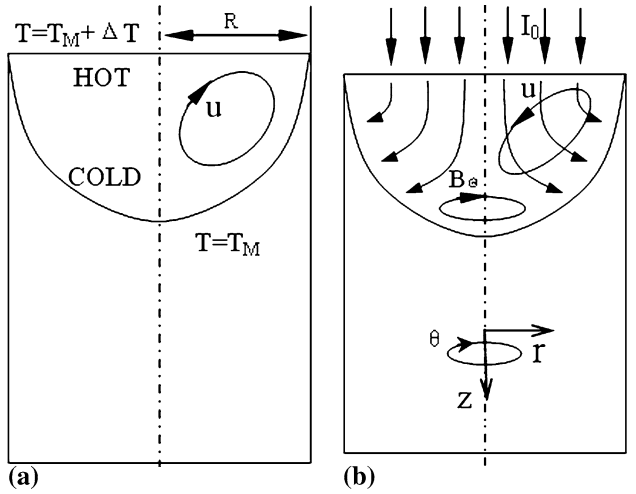

Fig. 5 Buoyancy and Lorentz of molten pool: (a) Buoyancy and (b) Lorentz $J \times B_\theta$ where B_θ is the self-field with current J

of the pool is contacted with the plasma arc and may be 200-300 K above the melting point of the alloy. Liquid metal at the surface will be hotter and less dense and so a buoyancy force would cause mixing because the molten pool is oval, i.e., the temperature difference will drive a buoyancy flow which points to the solidification front and leads the edge of liquid to the core of molten pool, as illustrated in Fig. 5(a). The case will facilitate the accord of temperature in the whole molten pool and mitigates the macrosegregation degree of ingots.

The second source of motion is the Lorentz force. The type of current path of the furnace is coaxial. The current flow I through the pool is related to the field B by Ampere's law, according to which

$$\nabla \times B = \mu J \qquad \text{(Eq 5)}$$

$$\nabla \times B = \left(\frac{1}{r}\frac{\partial B_z}{\partial \theta} - \frac{\partial B_\theta}{\partial z}\right)\hat{\hat{e}}_r + \left(\frac{\partial Br}{\partial z} - \frac{\partial Bz}{\partial r}\right)\hat{e}_\theta + \left(\frac{1}{r}\frac{\partial (rB_\theta)}{\partial r} - \frac{1}{r}\frac{\partial Br}{\partial \theta}\right)\hat{e}_z \qquad \text{(Eq 6)}$$

The magnetic field comes mainly from z direction melting current, and using Eq 6, we may rewrite as

$$\nabla \times B = -\frac{\partial B_\theta}{\partial z}\hat{e}_r + \frac{1}{r}\frac{\partial (rB_\theta)}{\partial r}\hat{e}_z \qquad \text{(Eq 7)}$$

$$\mu J_z = \frac{1}{r}\frac{\partial (rB_\theta)}{\partial r}\hat{e}_z \qquad \text{(Eq 8)}$$

So the Lorentz force which arises from the current flow and self-induced magnetic field can be expressed as

$$F_1 = J_Z B_\theta \qquad \text{(Eq 9)}$$

From Eq 8 and 9, Lorentz force can be written as

$$F_1 = B_\theta \frac{1}{r}\frac{\partial (rB_\theta)}{\mu \partial r}\hat{e}_z \qquad \text{(Eq 10)}$$

The Lorentz force F_1 comes into being a counter-clockwise flow cell, as shown in Fig. 5(b), which result in liquid transferring from the top to the core and brings lots of heat from the surface to the bottom of the pool. Finally, the molten pool becomes much deeper and the zone of liquid-solid two-phase becomes broader with the melting current increasing, which enhances the degree of convection and aggravates the macrosegregation degree of ingots.

In VAR, the fluid flow pattern is the resultant of the interaction between the thermal buoyancy forces and the electromagnetic Lorentz force. In general, buoyancy forces dominate at a low current operation. As the current is gradually increased, the influence of the electromagnetic Lorentz forces begins increasing (Ref 19). The value of buoyancy forces and the electromagnetic Lorentz force is close and the transition from buoyancy driven flow to current induced flow is very rapid in VAR process (Ref 20). Zanner (Ref 21) finds that when the melting current changes from 6.6 kA to 7.6 kA for remelting 508 mm diameter INCOEL718 alloy, the flow pattern between the thermal buoyancy forces and the electromagnetic Lorentz force has transformed in VAR. Davidson (Ref 15) studies that the flow pattern has transformed for remelting 250 mm diameter nickel alloy by numerical experiments. At melting current is 3.6 kA, the buoyancy dominates flow pattern, but melting current reaches 10 kA, the buoyancy driven motion has completely disappeared and the electromagnetic Lorentz force dominates flow pattern.

The researchers have divarication for critical value melting current which leads to transform the flow pattern in molten pool, but it is out of question that the electromagnetic Lorentz force increases with the increase of melting current and the effect of buoyancy forces and electromagnetic Lorentz force is opposite. At one time, macrosegregation formation tendency becomes significant with the increase of the electromagnetic Lorentz force. Therefore, in Ti-10V-2Fe-3Al alloy VAR process, the melting current of 1.7 kA generates relative small Lorentz force and the liquid flow of pool is dominated by the buoyancy force, which leads to the macrosegregation rate of alloying element decreases. But the higher melting current (2.6 kA) will result in a strong electromagnetically driven flow, therefore, the molten pool becomes very deep due to the drop of metal liquid increasing in unit time, and the dendrite at the front of S/L interface is washed and consequently, the enriched Fe element between interdendrite can be transferred to the center of the pool, which ultimately aggravates macrosegregation degree of ingots.

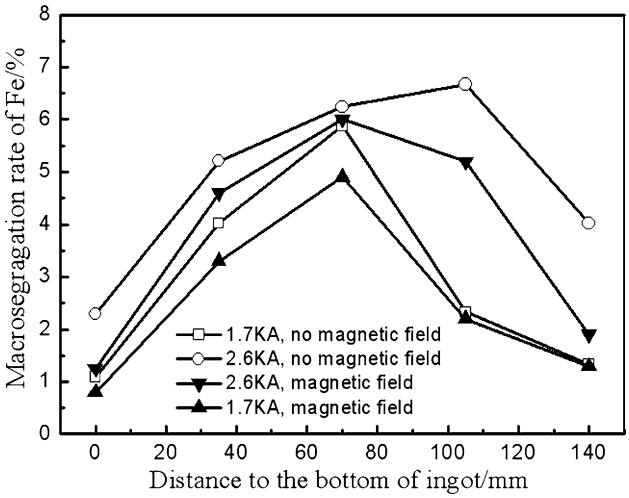

Fig. 6 Effect of magnetic field on macrosegregation rate of Fe element in ingots

So the macrosegregation of Fe element is bigger with 2.6 kA melting current than that with 1.7 kA, as shown in Fig. 4.

3.3 Influence of Magnetic Field on the Macrosegregation of Ti-10V-2Fe-3Al

Stirring magnetic field plays the important role in VAR process, and the effect of magnetic field on macrosegregation rate of Fe element in Ti-10V-2Fe-3Al ingots is shown in Fig. 6. It is found that when the melting current is the same such as 1.7 and 2.6 kA, the macrosegregation rate of Fe element decreases when the alloy is remelted with magnetic stirring compared with without magnetic stirring.

With magnetic stirring in VAR process, as shown in Fig. 7(a) and (b), there is a vertical magnetic field B_0 and it is introduced to stabilize the arc. The interaction of B_0 with the radial current in the pool gives rise to an azimuthal force which induces swirl, namely motion in a horizontal plane. It is the third source of force in the pool of VAR, as shown in Fig. 7(c). Expression of the force can be expressed as:

$$F_b = -B_0 \frac{\partial B_\theta}{\mu \partial z} e_r \qquad \text{(Eq 11)}$$

Magnetic stirring force intensify the convection of molten metal, which results in the crystal metal remelting at the brim of ingots. Thereby, the temperature difference of molten metal becomes small in VAR pool and becomes uniformity. So the zone of liquid-solid two-phase becomes narrow and the temperature gradient becomes higher at the front of S/L interface, which induces partition coefficient K_0 becomes larger. Ban et al. (Ref 22) discovers homoplastic phenomenon that direct magnetic field makes partition coefficient K_0 become larger in Al-Cu alloy. That is to say, magnetic field can meliorate the macrosegregation of alloying element, namely the macrosegregation rate of Fe element decreases in Ti-10V-2Fe-3Al ingots. Therefore, to prevent segregation during VAR, it is efficiently to adopt small melting current and bring to bear magnetic stirring (such as ingot B).

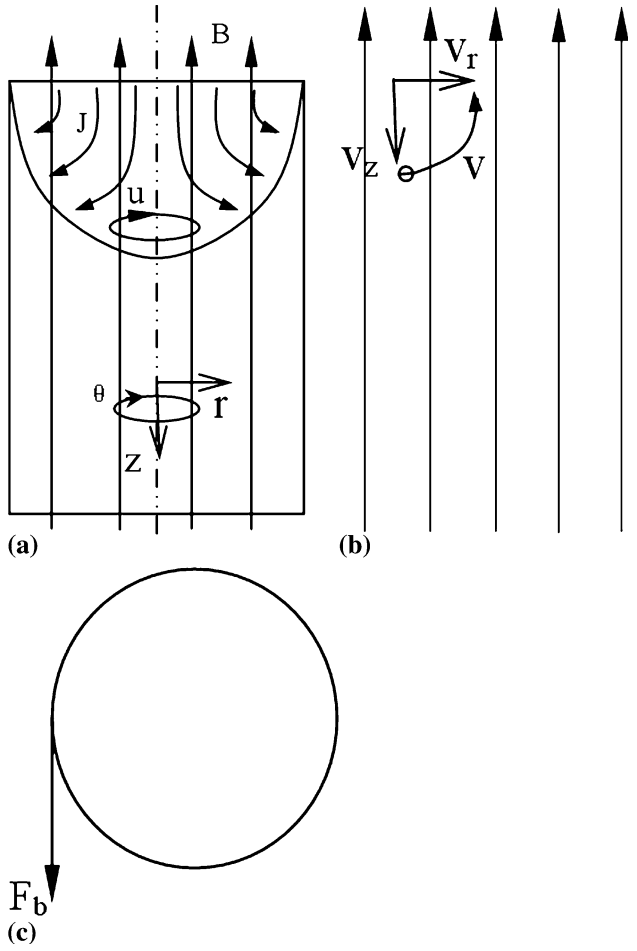

Fig. 7 Buoyancy and Lorentz of molten pool: (a) Lorentz $J \times B_0$ where B_0 is an externally field, (b) the movement of electron in magnetic field, and (c) azimuthal force in horizontal direction

4. Conclusion

1. In VAR process, the Fe content gradually increases along the axial direction from the bottom to the top of ingots and decreases along the radial direction from the center to the edge of ingot. The degree of macrosegregation is greater in the radial direction in the middle of the Ti-10V-2Al-3Fe ingot versus the top and bottom.
2. The macrosegregation rate increases firstly and then decreases along radial direction from the bottom to the top of the ingots with different melting currents. The macrosegregation rate of Fe element is higher with melting current of 2.6 kA than that of 1.7 kA in Ti-10V-2Al-3Fe ingot.
3. Without magnetic stirring, there are two forces, buoyancy and Lorentz forces which arise from the passage of current through the pool of VAR. There are three forces in the pool, a new Lorentz force arose with magnetic stirring because the presence of external inductors. The macrosegregation rate of Fe element decreases when the alloy remelts with magnetic stirring compared with without magnetic stirring. In order to reduce segregation of Fe element in Ti-10V-2Al-3Fe alloy, it is efficient to adopt small melting current and bring to bear suitable magnetic stirring.

Acknowledgment

This work was supported by National Basic Research Program of China (973 Project) (No. 2007CB613802).

References

1. M. Alec, Melting and Refining of Superalloy and Titanium Alloys, *ISIJ Int.*, 1992, **32**, p 557–562
2. K.S. Chan, L. Perocchi, and G.R. Leverant, Constitutive Properties of Hard-Alpha Titanium, *Metall. Mater. Trans.*, 2000, **A31**, p 3029–3040
3. H. Hiroshi, F. Nobuo, U. Takeshi, K. Masaaki, G.S. Hirowo, and F. Takashi, Solidification Structure and Alloy Produced by Vacuum Segregation in Cast Ingots Arc Consumable Electrode of Titanium Method, *ISIJ Int.*, 1991, **31**, p 775–784
4. Y. Akihiro and I. Hiroyuki, Dissolution of Refractory Elements to Titanium Alloy in VAR, *ISIJ Int.*, 1992, **32**, p 600–606
5. R.M. Ward and M.H. Jacobs, Electrical and Magnetic Techniques for Monitoring Arc Behaviour During VAR of INCONEL 718: Results from Different Operating Conditions, *J. Mater. Sci.*, 2004, **39**, p 7135–7143
6. P.D. Lee, A. Mitchell, A. Jardy, and J.P. Bellot, Liquid Metal Processing and Casting, *J. Mater. Sci.*, 2004, **39**, p 7133
7. A. Mitchell, Melting, Casting and Forging Problems in Titanium Alloys, *Mater. Sci. Eng.*, 1998, **A243**, p 257–262
8. J.P. Bellot, B. Foster, S. Hans, E. Hess, D. Ablitzer, and A. Mitchell, Dissolution of Hard-Alpha Inclusions in Liquid Titanium Alloys, *Metall. Mater. Trans.*, 1997, **B28**, p 1001–1001
9. V.I. Dobatkin and N.F. Anoshkin, Comparison of Macrosegregation in Titanium and Aluminium Alloy Ingots, *Mater. Sci. Eng.*, 1999, **A263**, p 224–229
10. R.L. Williamson, J.J. Beaman, D.K. Melgaard, G.J. Shelmidine, A.D. Patel, and C.B. Adasczik, A Demonstration of Melt Rate Control During VAR of "Cracked" Electrodes, 2004. Liquid Metal Processing and Casting, *J. Mater. Sci.*, 2004, **39**, p 7161–7169
11. W.D. Zeng and Y.G. Zhou, Effect of Beta Flecks on Mechanical Properties of Ti–10V–2Fe–3Al Alloy, *Mater. Sci. Eng.*, 1999, **A260**, p 203–211 (in Chinese)
12. G. Brian, Thomas and L.F. Zhang, Mathematical Modeling of Fluid Flow in Continuous Casting, *ISIJ int.*, 2001, **41**, p 1181–1193
13. D.G. Eskin, R. Nadella, and L. Katgerman, Effect of Different Grain Structures on Centerline Macrosegregation During Direct-Chill Casting, *Acta Mater.*, 2008, **56**, p 1358–1365
14. J.W. Christian, *The Theory of Transformation in Metals and Alloys*, 3rd ed., University of Oxford, UK, 1981, p 667–670
15. P.A. Davidson, X. He, and A.J. Lowe, Flow Transitions in Vacuum Arc Remelting, *J. Mater. Sci. Technol.*, 2000, **16**, p 699–712
16. Y.Q. Zhao, J.L. Liu, and L. Zhao, Segregation of Ti-2.5Cu, Ti-3Fe and Ti-3Cr Alloy Ingots, *Rare Met. Mater. Sci. Eng.*, 2004, **33**, p 731–735 (in Chinese)
17. Y.Q. Zhao, J.L. Liu, and L. Zhao, Analysis on the Segregation of Typical β Alloying Elements of Cu, Fe and Cr in Ti Alloys, *Rare Metal Mater. Sci. Eng.*, 2005, **34**, p 531–538 (in Chinese)
18. J.L. Liu, Y.Q. Zhao, and L. Zhao, Segregation of Ti-2.5Cu, Ti-3Fe and Ti-3Cr Alloy Ingots, *Rare Metal. Mater. Sci. Eng.*, 2004, **33**, p 731–735 (in Chinese)
19. D. Zagrebelnyy, M. John, and M. Krane, Segregation Development in Multiple Melt Vacuum Arc Remelting, *Metall. Mater. Trans.*, 2009, **B40**, p 281–288
20. L.A. Bertram, C.B. Adasczik, D.G. Evans, R.S. Minisandram, P.A. Sackinger, D.D. Wegman, and R.L. Williamson, *Symposium on Liquid Metal Processing and Casting*, A. Mitchell and P. Auburtin, Ed., Santa Fe, NM, Feb 16-19, 1997, American Vacuum Society, New York, NY, 1997, p 110–132
21. F.J. Zanner, R.L. Williamson, R.P. Harrison, H.D. Flanders, R.D. Thompson, and W.C. Szeto, *Superalloy 718-Metallurgy and Application*, E.A. Loria, Ed., TMS, Warrendale, PA, 1989, p 17–32
22. C.Y. Ban, J.Z. Cui, Q.X. Ba, G.M. Lu, and B.J. Zhang, The Influence of Pulsed Magnetic Field on Microstructures and Macrosegregation in 2124 Al-Alloy, *Acta Metall. Sin.*, 2002, **15**, p 380–384